IMAGE ANALYSIS FOR DETECTION OF CORONARY ARTERY SOFT PLAQUES IN MDCT IMAGES

Félix Renard[1] and Yongyi Yang[2]

[1]*LSIIT, UMR ULP-CNRS 7005, Strasbourg, France*

[2]*Department of Electrical and Computer Engineering*
Illinois Institute of Technology, Chicago, IL 60616, USA

Abstract

In this paper we aim to develop a computationally-efficient image-segmentation procedure for detection and quantification of soft plaques in coronary arteries from multidetector CT images. The proposed method consists of three steps: extraction of the arterial lumen centerline, segmentation of the lumen and arterial wall separately with locally adaptive region growing, and detection of soft plaques based on effective cross-section areas of the lumen and of the wall. Preliminary results using clinical acquisitions are presented to demonstrate the effectiveness of the proposed method.

Index Terms – Vulnerable plaque, vessel tracking, MDCT images, image segmentation

1. Introduction

Studies in recent years have indicated that the rupture of artery lesions known as vulnerable plaques is a major cause of heart attacks [1,2]. Consequently, there is great interest in developing imaging techniques for detection and identification of vulnerable plaques in patients. Multidetector CT (MDCT) recently has emerged as a promising tool for characterization of atherosclerotic plaque composition and morphology within the coronary arteries [3-5].

In this paper, we aim to develop an image segmentation and analysis procedure for identifying soft plaques in coronary arteries from MDCT image data. In the literature there exists a great deal of work on segmentation and visualization of blood vessels in various organs with different modalities (e.g., see [6] for a detailed review). Most of these methods, if not all, focus on how to extract vascular structures from image data.

Unlike calcified plaques, soft plaques exhibit as low intensity and have very little contrast from the arterial wall inside which they reside. Moreover, the vessel may not always exhibit narrowing at soft plaque site; on the contrary, it may even undergo positive remodeling [1]. This consequently poses a significant challenge for soft plaque identification in the presence of imaging noise, as a traditional approach simply based on lumen narrowing analysis no longer works well. Our goal in this work is to demonstrate the feasibility of applying image analysis on both the lumen and arterial wall for detection and quantification of soft plaques from MDCT data.

In this feasibility study, we will focus on a procedure that is computationally efficient, which is critical for practical implementation because modern MDCT scanners can now produce large volumes of data with ever reduced imaging time.

Since soft plaques are known to lie within the arterial wall [2], our procedure begins with segmentation of the major coronary arteries, which includes separate segmentation of the lumen and arterial wall. We then identify the presence of soft plaques by examining the geometric and image features of the lumen and its surrounding wall surfaces. Our results using clinical acquisitions demonstrate that this procedure can produce reliable results in the presence of both calcified and soft plaques, which is important for subsequent analysis of soft plaques.

2. Methods

Our proposed procedure consists of the following three steps: 1) detect the centerline of the arterial lumen by using a multi-scale vessel tracking algorithm, 2) segment out separately the lumen and wall of the arteries by applying adaptive region-growing, and 3) identify presence of soft plaques by differentially comparing the cross-sectional areas of the detected lumen and wall. These steps are explained below.

2.1. Centerline extraction

With contrast enhancement the lumen voxels of the coronary arteries appear brighter than their immediate surroundings, and as a consequence the blood vessels can be modeled by a tubular structure in MDCT images. As mentioned earlier, there are many methods developed in the literature for vessel tracking based on this property (e.g., [7]). Out of consideration of computation complexity, we adopt a centerline tracking approach that is similar in spirit to [8], where

vessel tracking is guided by a multi-scale filter based on local eigenvalue analysis of the Hessian matrix of the image.

To guard against possible leakage of the tracking direction away from the lumen caused by presence of nearby disturbances, e.g., myocardial cavities or calcified plaques in the arteries, we first apply a pre-processing step to isolate these disturbance factors. In addition, we also introduce an autoregressive filtering step on the estimated local lumen direction to suppress the impact of imaging noise. Our results show that this can improve the robustness of the tracking algorithm.

2.1.1. Multi-scale centerline tracking. The tracking procedure starts with a seed point $\mathbf{p}_0$ selected on the lumen of a coronary artery, and searches for a set of centerline points along the path of the lumen in the following successive fashion: at point $\mathbf{p}_i$, $i = 0,1,\cdots$,

a. Refine the point $\mathbf{p}_i$ so that it lies on the centerline of the lumen.
b. Perform multi-scale Hessian filter analysis to obtain the local principal direction $\mathbf{v}_i$ of the lumen at $\mathbf{p}_i$.
c. Search for the next point along direction $\mathbf{v}_i$, i.e., $\mathbf{p}_{i+1} = \mathbf{p}_i + d_i\mathbf{v}_i$, where d_i is the step size.
d. Repeat the above steps until the stop criterion is met.

2.1.2. Centerline points and vessel direction. Since the lumen voxels are brighter than their surroundings, the centerline point $\mathbf{p}_i$ is estimated by using the local center of gravity of the lumen (step a above) [8]. Specifically, at $\mathbf{p}_i$ we update it by computing the center of gravity of an image window centered around $\mathbf{p}_i$. We iterate this until the change between two successive estimates is within a prescribed range (e.g., less than one voxel).

To determine the principal direction $\mathbf{v}_i$ at centerline point $\mathbf{p}_i$, we use the vesselness measure by Frangi *et al.* [9]. Specifically, at $\mathbf{p}_i$ we compute the Hessian matrix $\mathbf{H}$ of the image convolved with a Gaussian kernel with scale factor σ. We then compute the eigenvalues/eigenvectors of the matrix $\mathbf{H}$, based on which the vesselness measure $V(\mathbf{p}_i,\sigma)$ is computed. This measure is computed for different values of σ, and the best match with the vessel is selected based on the largest value of $V(\mathbf{p}_i,\sigma)$. The properties of the eigenvalues of $\mathbf{H}$ give important information about the vessel structure at $\mathbf{p}_i$, such as tubular vs plate-like structure (at vessel bifurcation); moreover, the eigenvector associated with the smallest eigenvalue (in magnitude) corresponds to the principal direction of the vessel, and the other two eigenvectors correspond to the cross-section of the vessel.

It is expected that the estimated principal direction above will be sensitive to the imaging noise, because the Hessian matrix $\mathbf{H}$ involves the second derivatives of the image. To reduce the impact of the noise, we apply a post-filtering step on the search direction vector. Specifically, let $\mathbf{v}_i'$ denote the computed principal direction at $\mathbf{p}_i$ from eigenvalue analysis as above. Then the search direction $\mathbf{v}_i$ is obtained by using the following autoregressive filter:

$$\mathbf{v}_i = \alpha\mathbf{v}_i' + (1-\alpha)\mathbf{v}_{i-1} \qquad (1)$$

where $\mathbf{v}_{i-1}$ is the search direction at previous centerline point $\mathbf{p}_{i-1}$, $0 < \alpha < 1$ is a constant used to control the update speed. In our experiments, $\alpha = 0.5$ was used.

To avoid backward tracking, the eigenvector $\mathbf{v}_i'$ in (1) is chosen to be in the general direction of $\mathbf{v}_{i-1}$, i.e., $\langle \mathbf{v}_i', \mathbf{v}_{i-1} \rangle > 0$; otherwise, its opposite direction is used.

In our experiments, for centerline extraction a cubic window with 10 voxels in each dimension was used for computing the center of gravity; the step size used was 3 pixels between two consecutive centerline points.

2.1.3. Pre-processing of images. As can be seen, the centerline searching procedure can be disturbed by image features that may exist in the local neighborhood of the arteries. This may happen when the vessel is in close vicinity of the myocardial cavities, or even when there are significant calcified plaques present in the arteries. To avoid these factors, we apply a pre-processing step to first segment out the nearby heart cavities and remove any relevant calcified voxels in the searching step.

With contrast enhancement, the heart cavities can be easily segmented out from its surrounding. In Fig. 1 we show an example, where the two cavity regions are segmented out by using a simple region-growing algorithm. In obtaining these results, a 10×10 seed region was selected, based on which the mean and standard deviation were computed and an interval was derived (within three times of the stand deviation from the mean) for region growing. Upon segmentation, these cavities regions were set to the same intensity level as the myocardium.

When present, the calcified voxels can be easily identified by examining their intensity values (which are close to that of bone). Thus, to reduce their impact, we can simply set these calcified voxels to a lower intensity (e.g., that of the seed point $\mathbf{p}_0$) when they are found to be inside the search window used for computing the center of gravity at a centerline point.

2.2. Arterial lumen and wall segmentation

2.2.1. Lumen segmentation. Upon examination of the image data, it is observed that the intensity value of lumen voxels would vary along the path of the vessel. This is especially true with the presence of either calcified or soft plaques. This indicates that the lumen voxels may not be modeled well by a constant region. To accommodate this variation, we adopt an adaptive region growing approach for segmentation of the lumen voxels.

Specifically, for each segment between two consecutive centerline points $\mathbf{p}_i$ and $\mathbf{p}_{i+1}$, we first determine the local statistical distribution of the lumen voxels by calculating the mean m_i and standard deviation σ_i of the intensity values from N centerline points that are immediately next to $\mathbf{p}_i$ and $\mathbf{p}_{i+1}$. Next, we compute a local threshold as $T_i = m_i - 2\sigma_i$. We then perform region growing with this threshold from seed point $\mathbf{p}_i$ to identify the lumen voxels between the two cross-section planes at centerline points $\mathbf{p}_i$ and $\mathbf{p}_{i+1}$, respectively. This process is repeated until the end of the centerline is reached. In our experiments, N=20 was used.

2.2.2. Wall segmentation. Since the lumen is immediately surrounded by the arterial wall, we first apply a morphological dilation operation on the detected lumen with a ball structuring element of radius R voxels. This is used to isolate those possible candidates for wall voxels. Let S denote the set of augmented voxels resulted from this dilation operation, which does not include the lumen voxels.

Next, we apply an adaptive region growing procedure to identify wall voxels from the set S. Specifically, for each segment between two consecutive centerline points $\mathbf{p}_i$ and $\mathbf{p}_{i+1}$, we calculate the mean m_i' and standard deviation σ_i' of the intensity values from those voxels in S that also lie between the two cross-section planes at $\mathbf{p}_i$ and $\mathbf{p}_{i+1}$. We then define a threshold $T_i' = m_i' - 3\sigma_i'$. Afterward, we perform region growing from the lumen segment between $\mathbf{p}_i$ and $\mathbf{p}_{i+1}$ by including only those voxels in S that have intensity values between T_i' and T_i. This process is repeated until the end of the centerline is reached.

We note that the region growing above is limited to only the set of voxels S augmented in the dilation step. This is to prevent the region growing step from leaking into the surrounding myocardium or even other nearby vessels. In our experiments, R=5 was found to be sufficient (which is close to the diameter of the lumen).

2.23. Identification of soft plaques. To quantify possible narrowing of the vessel caused by plaques, we compute the effective cross-section area of the lumen. This is obtained by dividing the volume of the lumen segment between two centerline points $\mathbf{p}_i$ and $\mathbf{p}_{i+1}$ by the distance between them. Let $A_l(i)$ denote this resulting area. In a similar fashion, we can compute the effective cross-section area of the identified arterial wall $A_w(i)$. This area measure can signal the presence of positive vessel remodeling.

Thus, by contrasting these two area measures $A_l(i)$ and $A_w(i)$, we obtain a measure that will signal the presence of either calcified or soft plaques. Specifically, we calculate the difference between the two measures $A_d(i) = A_w(i) - A_l(i)$.

3. Results and discussions

To demonstrate the proposed methods, we present results obtained with two sets of clinical acquisitions. The first dataset was from a subject which showed a small soft plaque in the left anterior descending (LAD) artery. The second dataset was from a subject with significant plaque load. Both datasets were acquired on a Philips 64-slice CT scanner. Each volume consisted of 300 slices of 512×512 images. The slice thickness was 0.45 mm, and the pixel size was 0.43 mm.

In Fig. 2 we show the results obtained for the first dataset, where Fig. 2a shows the extracted lumen of the LAD artery, in which a soft plaque is identified; Fig. 2b shows a cross-sectional view of the arterial wall of a segment in this artery; Fig. 2c show the intensity images for three cross sections on this segment, where section B corresponds to the soft plaque; Fig. 2d shows the cross-section areas of the lumen, wall, and their difference along the path of the artery. As can be seen, the extent of the soft plaque is clearly reflected in these cross-section curves.

Similarly, in Fig. 3 we show the results obtained with the second dataset, in which the left circumflex (LCX) artery is shown. As can be seen, there are multiple plaques, calcified and soft, present in this artery. In particular, cross section B in Fig. 3c shows a calcified plaque (indicated by the high intensity region). In addition, the cross sections A-C also show that this artery segment is in close vicinity of a myocardial cavity (indicated by high intensity regions). In Fig. 3d we show a maximum intensity projection (MIP) view of this artery (including both lumen and wall), which shows multiple calcified and soft plaques.

The proposed procedure could nevertheless still segment the artery correctly despite these local interferences. These detection results were confirmed by an experienced radiologist.

4. Conclusion

In this paper we developed a computationally efficient procedure based on image segmentation and analysis for identification of soft plaques in coronary arteries from MDCT images. The procedure consisted of the following three steps: 1) extraction of the lumen centerline by using a multi-scale vessel tracking filter, 2) segmentation of the lumen and wall separately by using locally adaptive region growing, and 3) quantification of soft plaques by examining the effective cross-section areas of the lumen and arterial wall. The proposed methods were demonstrated to be effective for identification of both calcified and soft plaques on real clinical acquisitions. Encouraged by these initial promising results, we plan to further develop and validate the proposed procedure with more comprehensive clinical evaluations.

References

[1] M. Madjid, A. Zarrabi, *et al*., "Finding vulnerable atherosclerotic plaques: Is it worth the effort?" Arteriosclerosis Thrombosis and Vascular Biology, vol. 24, pp.1775-1782, 2004.

[2] R. Virmani, A. P. Burke, A. Farb, F. D. Kolodgie, "Pathology of the vulnerable plaque," *J Am Coll Cardiol,* vol. 47, 2006.

[3] M. A. S. Cordeiro and J. A. C. Lima, "Atherosclerotic plaque characterization by multidetector row computed tomography angiography," *J Am Coll Cardiol*, vol. 47, pp.C40-47, 2006.

[4] S. Achenbach, F. Moselewski, *et al*., "Detection of calcified and noncalcified coronary atherosclerotic plaque by contrast-enhanced, submillimeter multidetector spiral computed tomography…," *Circulation*, vol. 109, pp.14-17, 2004.

[5] C. Toumoulin, C. Boldak, M. Garreau, D. Boulmier, "Coronary characterization in multi-slice computed tomography," *Computers in Cardiology,* vol. 30, pp. 749-752, 2003.

[6] C. Kirbas and F. Quek, "A review of vessel extraction techniques and algorithms," *ACM Comput. Surveys (CSUR)*, vol. 36, 2004.

[7] Y. Yang, A. Tannenbaum, D. Giddens, "Knowledge-based 3D segmentation and reconstruction of coronary arteries using CT images", *Proc. of 26th IEEE EMBS Annual Inter Conf*, 2004.

[8] G. Yang, A. Bousse, C. Toumoulin, H. Shu, "A multiscale tracking algorithm for the coronary extraction in MSCT angiography", *Proc. of 28th IEEE EMBS Annual Inter Conf*, 2006.

[9] A. Frangi, W. Niessen, *et al.*, "Multiscale vessel enhancement filtering," MICCAI'98, vol. 1496 of LNCS, pp. 130-137, 1998.

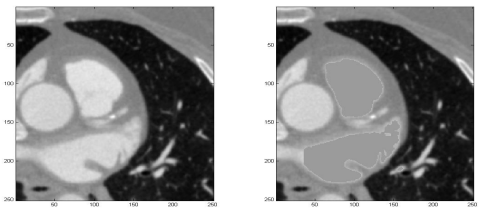

Fig. 1. *Left*: a 2D slice showing the heart region; *Right*: the same slice with two myocardial cavities segmented.

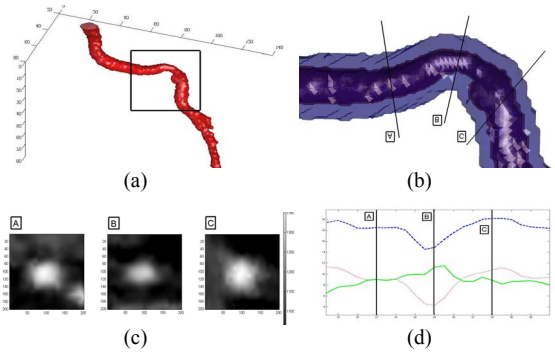

Fig. 2. Results from the first dataset: (a) extracted lumen of LAD artery, in which a soft plaque is present; (b) cross-sectional view of the arterial wall of a segment of this artery; (c) corresponding intensity images of different cross sections indicated in (b), where section B corresponds to the soft plaque; (d) effective cross-section areas of the lumen (dotted-red), wall (dashed-blue), and their difference (solid-green) along the artery path.

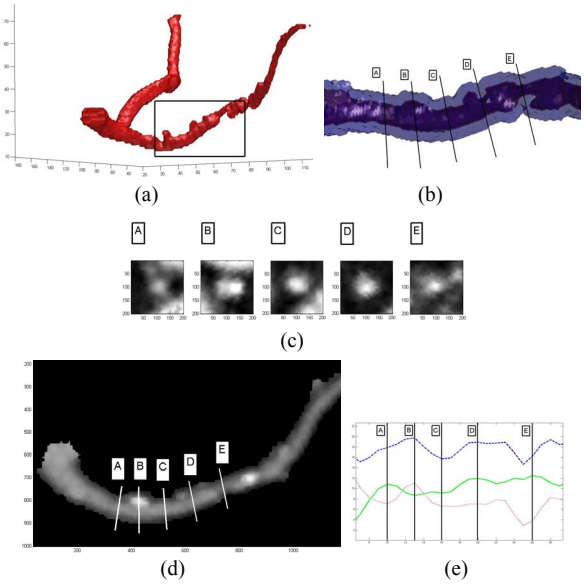

Fig. 3. Results from the second dataset: (a) extracted lumen of LCX artery, in which multiple plaques are present; (b) cross-sectional view of the arterial wall of a segment of this artery; (c) intensity images corresponding to different cross sections indicated in (b), where section B shows calcified plaque (reflected by the high intensity region), and sections A, D, and E show soft plaques; (d) MIP view of the LCX vessel (lumen and wall), which shows multiple calcified and soft plaques; (e) the effective cross-section areas of the lumen (dotted-red), wall (dashed-blue), and their difference (solid-green) along the artery path.